Electronic Supplementary Material (ESI) for Physical Chemistry Chemical Physics.

Electronic Supplementary Information

Theoretical Predication on the High Hydrogen Evolution Catalytic Activity for the Cubic and Tetragonal SnP Systems

Jingwei Liu, Guangtao Yu*, Ran Zhang, Xuri Huang*, Wei Chen*

Laboratory of Theoretical and Computational Chemistry, Institute of Theoretical Chemistry, Jilin University, Changchun 130023, People's Republic of China

*To whom correspondence should be addressed. Email: yugt@jlu.edu.cn (G.Y.), huangxr@jlu.edu.cn (X.H.), w_chen@jlu.edu.cn (W.C.)

(I) Possible exposed surfaces for the cubic and tetragonal SnP systems by Bravais–Friedel–Donnay–Harker (BFDH) crystal morphology algorithm

The Bravais-Friedel-Donnay-Harker (BFDH) method is a geometrical calculation that uses the crystal lattice and symmetry to generate a list of possible growth faces and their relative growth rates. From this, crystal morphology can be deduced. Based on the BFDH theory, the relative growth rates of faces {*hkl*} on crystals have a positive relationship with the center-to-face distance, which can be inversely proportional to the interplanar spacing.

$$R_{hkl} \propto D \propto 1/d$$

where R_{hkl} is the growth rate in the {*hkl*} plane, D is center-to-face distance and d is interplanar distance. Clearly, the lowest growing rates can occur at the faces with the largest interplanar spacing, all of which can be the most morphologically important.

Up to now, BFDH method has been extensively employed in predicting the morphology for various crystals[1-5]. Although the BFDH method does not take into account the energetics of studied systems, it can obtain a rough estimate of the faces that are likely to be important for the crystal habit. Particularly, this information can be used to pre-screen the face list used as an input to more sophisticated morphology calculations.

In this work, there are many surface terminations for the bulk SnP structures, and it is almost unpractical to calculate the surface energy of each surface[6]. According to the convention[7-9], therefore, we initially employ the BFDH crystal morphology algorithm to roughly estimate the possible exposed surfaces for two studied SnP systems, and then further measure stability of each termination for these surfaces by computing the surface energy (the correlative details on calculating the surface energy have been presented in the section (II) of ESI). As shown in Table S1, the (111) and (200) facets for cubic SnP structure as well as the (101), $(10\bar{1})$, (110), (002) and $(00\bar{2})$ surfaces for tetragonal SnP structure can possess the relative large interplanar distance in the range of 2.71~3.22 Å, much larger than those of other remaining surfaces for the respective bulk structure. Consequently, all these facets are the possible exposed surfaces for

both the studied SnP systems, in view of their relatively low growing rates. Figure 2 in the main text illustrates the indexed morphological drawing for the cubic and tetragonal SnP systems.

Table S1. The possible exposed surfaces for the cubic and tetragonal SnP systems as well as the corresponding interplanar distance and the calculated relative growth rate by using BFDH method.

Surfaces (hkl)	d_{hkl}(Å)	Calculated relative growth rates
cub-(111)	3.159	1.000
cub-(200)	2.736	1.155
tet-(101)	3.223	1.000
tet-(10$\bar{1}$)	3.223	1.000
tet-(110)	2.982	1.081
tet-(002)	2.982	1.081
tet-(00$\bar{2}$)	2.708	1.190

(II) Computational details on the surface energy for cubic and tetragonal SnP systems

In this study, we have performed the computations on the surface energy for the possible exposed facets (from BFDH method) of cubic and tetragonal SnP systems, by following the scheme employed in the previous study by Tian *et al*[10]. The following correlative methods for computing surface energy have been presented for the symmetric/asymmetric and stoichiometric termination.

For the symmetric and stoichiometric termination, the surface energy (γ) can be computed by the following equation:

$$\gamma = (E_{total} - nE_{bulk})/2A \qquad (1)$$

where γ is the surface energy of SnP facet, E_{total} is the total energy of the relaxed SnP surface slab (both the same terminations are relaxed at the same time), E_{bulk} is the energy of a bulk SnP formula unit, n is the number of SnP units in the slab, and A is the surface area of one side of the slab.

For the asymmetric and stoichiometric termination, the surface energy is initially understood as the sum of cleavage energy (E_{cle}) and relaxation energy (E_{rel}):

$$\gamma = (E_{cle} + E_{rel})/A \qquad (2)$$

Considering that the cleavage energies of two generated terminations from one cleavage can be supposed to be equal due to the similar electronegativity of P and Sn, we can obtain the cleavage energy of a stoichiometric slab by the following equation:

$$E_{cle} = (E_{unrelax} - nE_{bulk})/2 \qquad (3)$$

$E_{unrelax}$ is the total energy of the unrelaxed SnP slab.

For the asymmetric slab, it can be divided into two parts from the middle. Then the relaxation energy for two different terminations T1/T2 can be gotten by the following equations:

$$E_{rel}（T1） = E_{T1\text{-}relax} - E_{unrelax} \qquad (4)$$

$$E_{rel}（T2） = E_{T2\text{-}relax} - E_{unrelax} \qquad (5)$$

$E_{T1\text{-}relax}$ is the energy of the slab only with the up-half part relaxed, while $E_{T2\text{-}relax}$ is the energy of the slab only with the down half part relaxed.

Among all ten terminations studied in our work, the cub-SnP-(200), tet-SnP-(110), tet-SnP-(002) and tet-SnP-($00\bar{2}$) can belong to the symmetric and stoichiometric termination, and we employ the equation (1) to calculate the surface energy. All these four surfaces can be modeled by the corresponding stoichiometric SnP-slabs with twelve SnP-layers. During the computational process, the upper/bottom two layers in the models are fully relaxed without any symmetry or direction restrictions, while the remaining layers are kept frozen. The six remaining terminations can belong to the asymmetric and stoichiometric terminations, including cub-P-(111), cub-Sn-(111), tet-P-(101), tet-Sn-(101), tet-P-($10\bar{1}$) and tet-Sn-($10\bar{1}$). The equations (2)~(5) are adopted to calculate their surface energies. The surfaces can be modeled by the corresponding stoichiometric SnP-slabs with twelve Sn/P-layers. During the computational process, the half part (six layers) in the models is fully relaxed without any symmetry or direction restrictions, while the remaining half part is kept frozen.

As shown in Table S2, the orders of computed surface energies are cub-P-(111) (γ = 0.787) ≈ cub-SnP-(200) (0.785) < cub-Sn-(111) (1.068) for the cubic SnP system

and tet-P-($10\bar{1}$) (γ=0.646) < tet-P-(101) (0.798) ≈ tet-SnP-(110) (0.777) < tet-Sn-($10\bar{1}$) (0.950) ≈ tet-SnP-(002) (0.966) ≈ tet-SnP-($00\bar{2}$) (0.970) < tet-Sn-(101) (1.149) for the tetragonal SnP system, respectively. Clearly, for both the cubic and tetragonal SnP systems, the P-terminated surface can be more stable than the corresponding Sn-terminated surface, in view of the more favorable surface energy. Additionally, the cub-P-(111) and cub-SnP-(200) can be the most stable surfaces for cubic SnP structure, while tet-P-($10\bar{1}$) is the most stable surface for tetragonal SnP structure, due to the lowest surface energy.

Table S2. The computed surface energies (γ) for the cub-P-(111), cub-Sn-(111) and cub-SnP-(200) surfaces for the cubic SnP system as well as the tet-P-(101), tet-Sn-(101), tet-P-($10\bar{1}$), tet-Sn-($10\bar{1}$), tet-SnP-(110), tet-SnP-(002) and tet-SnP-($00\bar{2}$) surfaces for the tetragonal SnP system.

Terminations	γ (J/m^2)
cub-P-(111)	0.787
cub-SnP-(200)	0.785
cub-Sn-(111)	1.068
tet-P-($10\bar{1}$)	0.646
tet-SnP-(110)	0.777
tet-P-(101)	0.798
tet-Sn-($10\bar{1}$)	0.950
tet-SnP-(002)	0.966
tet-SnP-($00\bar{2}$)	0.970
tet-Sn-(101)	1.149

(III) The illustration on the computational detail on ΔG_{H^*} for the second H adsorbed on the sampled cub-P-(111) surface

In this study, we have computed the ΔG_{H^*} values at the different surface coverages, where the adsorption order of H* can be decided in terms of energy. For example, on

the sampled cub-P-(111) surface with T_P serving as the HER active site, we consider both the possible adsorption sites (*i.e.* T_{P-2} and $T_{P-2'}$) for the second H to occupy, after the first H* is adsorbed at the T_{P-1}, as illustrated in the Figure S1. Our computed results reveal that the T_{P-2} site (-0.265 eV) can exhibit more negative ΔG_{H^*} value than the $T_{P-2'}$ site (-0.194 eV), indicating the stronger adsorption of the former than the latter. Thus, when computing the surface coverage, the second H* will be adsorbed at T_{P-2} site on cub-P-(111), in view of the more favorable adsorption energy. The similar mode has been also adopted for all the computations on the surface coverage in this work.

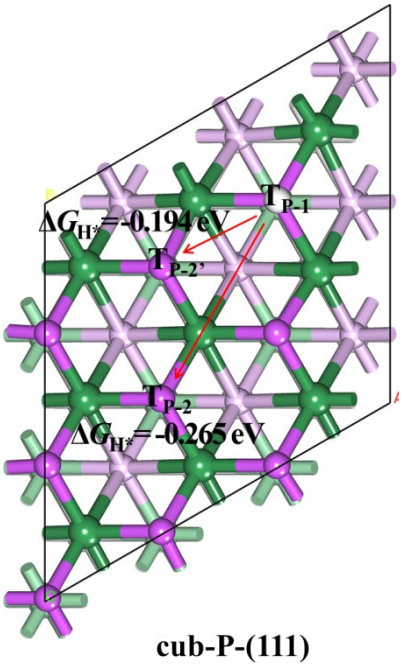

Figure S1. Two possible adsorption sites (T_{P-2} and $T_{P-2'}$) for the second H* on cub-P-(111).

(IV) The examination of solvation effect on the HER catalytic activity.

Based on the correlative structural models, we have explored the HER catalytic activity for all the sampled systems (including cub-P-(111), cub-Sn-(111), cub-SnP-(200), tet-P-(101), tet-Sn-(101), tet-P-($10\bar{1}$), tet-Sn-($10\bar{1}$) and tet-SnP-(110)) in solvation (Figure S2) and in vacuum to examine the solvation effect, by computing ΔG_{H^*} values of T_P and T_{Sn} sites. The computed results are presented in Table S3. It can be found that all the computed ΔG_{H^*} values are almost no change (< 0.069 eV) between the two situations, indicating the negligible solvation effect. Therefore, to

make the computational cost less demanding, in this study we compute ΔG_{H^*} value in the vacuum condition for estimating the HER activity for all the studied systems.

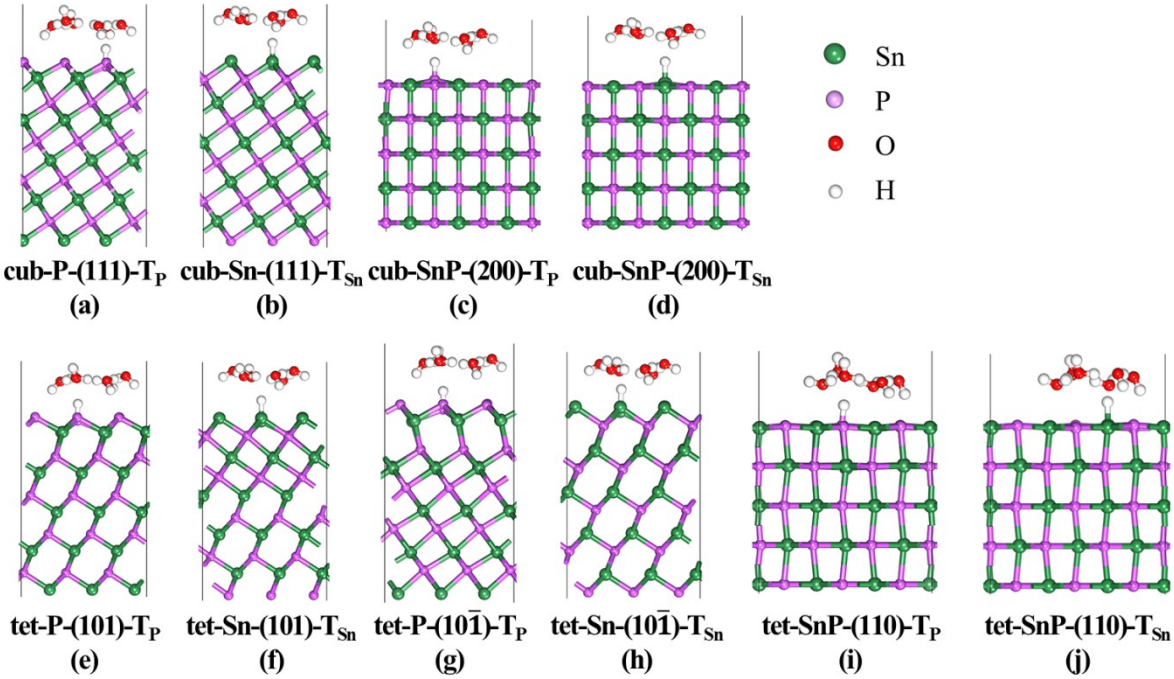

Figure S2 The side view of correlative geometrical structures with the adsorbed H* on the surface with a water layer above.

Table S3 The computed ΔG_{H^*} values in solvation and in vacuum for T_P and T_{Sn} sites on the sampled surfaces including cub-P-(111), cub-Sn-(111) and cub-SnP-(200) as well as tet-P-(101), tet-Sn-(101), tet-P-(10$\bar{1}$), tet-Sn-(10$\bar{1}$) and tet-SnP-(110).

Adsorption site	ΔG_{H^*}（eV）	
	vacuum	water
cub-P-(111)-T_P	-0.246	-0.309
cub-Sn-(111)-T_{Sn}	0.735	0.766
cub-SnP-(200)-T_P	0.250	0.221
cub-SnP-(200)-T_{Sn}	0.713	0.689
tet-P-(101)-T_P	-0.211	-0.243
tet-Sn-(101)-T_{Sn}	0.782	0.755
tet-P-(10$\bar{1}$)-T_P	-0.003	-0.045
tet-Sn-(10$\bar{1}$)-T_{Sn}	0.656	0.648
tet-SnP-(110)-T_P	0.222	0.291
tet-SnP-(110)-T_{Sn}	0.633	0.689

Reference:

1. Y. Yang, G. Liu, J. Liu, M. Wei, Z. Wang, X.-T. Hao, D. M. Repaka, R. V. Ramanujan, X. Tao and W. Qin, *ACS Appl. Mater. Interfaces,* 2018, **10**, 44654−44659.
2. X. Fang, X. Yang and D. Yan, *J. Mater. Chem. C*, 2017, **5**, 1632-1637.
3. F. Zasada, J. Grybos, P. Indyka, W. Piskorz, J. Kaczmarczyk and Z. Sojka, *J. Phys. Chem. C*, 2014, **118**, 19085-19097.
4. S. Bhukkal, N. Sinha, H. Yadav, S. Goel, B. Singh, I. Bdikin and B. Kumar, *Vacuum*, 2018, **154**, 90-100.
5. S. Goel, N. Sinha, H. Yadav, A. J. Joseph, A. Hussain and B. Kumar, *Arabian Journal of Chemistry*, 2017, 10.1016/j.arabjc.2017.03.003.
6. J. Kibsgaard, C. Tsai, K. Chan, J. D. Benck, J. K. Nørskov, F. Abild-Pedersen and T. F. Jaramillo, *Energy Environ. Sci.*, 2015, **8**, 3022-3029.
7. M. A. Fusella, F. Schreiber, K. Abbasi, J. J. Kim, A. L. Briseno and B. P. Rand, *Nano let.*, 2017, **17**, 3040-3046.
8. Y. Yuan and Z. Li, J. *Alloy. Compd*., 2018, **738**, 379-393.
9. Z. Zhang, G. Yu, H. Li, J. Liu, X. Huang and W. Chen, *Phys. Chem. Chem. Phys*., 2018, **20**, 10407-10417.
10. X. Tian, T. Wang, L. Fan, Y. Wang, H. Lu and Y. Mu, *Appl. Surf. Sci.*, 2018, **427**, 357-362.